

Reactive Rayleigh-Taylor Turbulence

M. Chertkov¹, V. Lebedev^{1,2}, and N. Vladimirova^{1,3,4}

¹ Theoretical Division & CNLS, LANL, Los Alamos, NM 87545, USA

² Landau Institute for Theoretical Physics RAS

³ ASC Flash Center, University of Chicago, 5640 S Ellis Ave, Chicago, IL 60637, USA

⁴ Department of Mathematics and Statistics, UNM, Albuquerque, NM 87131, USA

(Received 2 February 2022)

The Rayleigh-Taylor (RT) instability develops and leads to turbulence when a heavy fluid falls under the action of gravity through a light one. We consider this phenomenon accompanied by a reactive transformation between the fluids, and study with Direct Numerical Simulations (DNS) how the reaction (flame) affects the turbulent mixing in the Boussinesq approximation. We discuss “slow” reactions where the characteristic reaction time exceeds the temporal scale of the RT instability, $\tau \gg t_{\text{inst}}$. In the early turbulent stage, $t_{\text{inst}} \lesssim t \lesssim \tau$, effects of the flame are distributed over a maturing mixing zone, whose development is weakly influenced by the reaction. At $t \gtrsim \tau$, the fully mixed zone transforms into a conglomerate of pure-fluid patches of sizes proportional to the mixing zone width. In this “stirred flame” regime, temperature fluctuations are consumed by reactions in the regions separating the pure-fluid patches. This DNS-based qualitative description is followed by a phenomenology suggesting that thin turbulent flame is of a single-fractal character, and thus distribution of the temperature field is strongly intermittent.

1. Introduction

The Rayleigh-Taylor (RT) instability (Rayleigh 1883; Taylor 1950; Chandrasekhar 1961) occurs in many natural and man-made flows. Under constant acceleration, produced e.g. by gravity, the instability develops into the RT turbulence (Duff *et al.* 1962; Sharp 1984), characterized by a mixing zone which continuously grows. Many recent experimental (Dalziel *et al.* 1999; Wilson & Andrews 2002), numerical (Young *et al.* 2001; Dalziel *et al.* 1999; Cook & Dimotakis 2001; Ristorcelli & Clark 2004; Cabot & Cook 2006; Vladimirova & Chertkov 2008) and theoretical efforts (Chertkov 2003; Chertkov *et al.* 2005) — later ones in the spirit of the turbulence phenomenology (Kolmogorov 1941; Obukhov 1949; Corrsin 1951; Frisch 1995) — have been devoted to analysis of turbulence inside the mixing zone. The mixing fluids can also be involved in chemical or nuclear reactions, e.g. flame. A flame front propagating against the acceleration is modified by the RT instability, which leads to a reactive turbulence in the mixing zone. Studies of the externally stirred turbulent flames belong to the general field of turbulent combustion (Damköler 1940; Williams 1985; Peters 2000; Poinot & Veynante 2005; Borghi 1988; Kerstein 2001) and have many important applications. The buoyancy driven, reactive turbulence is believed to be the dominant mechanism for thermonuclear burning in type-Ia supernovae (Khokhlov 1995; Gamezo *et al.* 2003; Zingale *et al.* 2005). The interplay of buoyancy, reactive transformation and turbulence also plays a crucial role in studies of fusion (Freeman *et al.* 1977) and large-scale combustion, such as furnaces and fires (Cetegen & Kasper 1996; Tieszen 2001). Turbulence, generated by buoyancy,

facilitates mixing, and thus counteracts the dynamical separation of fluids (phases) due to reaction. To explain this competition between **separation and mixing** is the main challenge emerging in the description of reactive flows (Kerstein 2001), which also applies in the broader context of multi-phase fluid mechanics, e.g. the RT turbulence of an immiscible mixture controlled by surface tension (Chertkov *et al.* 2005).

To clarify the nature of the competition between separation and mixing, let us consider a typical reactive RT setting. Initially, the heavy, cold reactant is placed on top of the light, hot product. As in the non-reacting RT instability, the mixing zone develops. Since locally the reaction occurs only in the mixed fluid, turbulence inside the mixing zone enhances the cumulative reaction rate. The effect of reaction, however, is the opposite – the reaction consumes mixed material, and potentially limits the growth of the mixing zone. While diffusion and turbulence mix the reactant with the product, the reaction converts the mixed fluid into the product, thus causing an upward shift of the mixing zone as a whole.

Existing studies of reactive RT setting have mainly focused on the initial stages of instability (Lima *et al.* 2006), or on the instability restricted by container walls in experiments (Bockmann & Muller 2004) and by domain sizes in simulations (Khokhlov 1995; Zingale *et al.* 2005; Vladimirova & Rosner 2005). The transverse (to direction of gravity) confinement results in a constant (on average) cumulative reaction speed, presumably dependent on the domain size (Khokhlov 1995). In this system fluctuations, e.g. in velocity and density fields, do not grow with time. It is still not clear whether reaction can stabilize the unconfined RT instability. One suspects that the answer might depend on the relation between the timescale of the RT instability and the reaction timescale.

In this paper, we study RT turbulence unconfined by walls in the presence of reactions slower than RT instability. Armed with DNS and building a unifying phenomenological description, we analyze the interplay of turbulent mixing and reaction-mediated separation. Specifically, we focus on predicting macroscopic and microscopic features of the mixing zone, such as the upward transport of the mixing zone as a whole and statistics of density fluctuations within the mixing zone.

We examine the interacting effects of buoyancy and reaction in the simplest, however physically relevant setting, the Boussinesq approximation, where the variations in the fluid density are small and are related linearly to the temperature contrast. We assume that the pressure increase due to reaction is negligible, and that the Mach number is small and, consequently, the fluid is incompressible. Thus, our system can be modeled by the incompressible Navier-Stokes equation coupled to the advection-reaction-diffusion equation governing the temperature evolution. The set of equations is written as

$$\partial_t \mathbf{v} + (\mathbf{v} \nabla) \mathbf{v} = -\nabla p + \nu \nabla^2 \mathbf{v} - 2\mathcal{A}g\theta, \quad \nabla \cdot \mathbf{v} = 0, \quad (1.1)$$

$$\partial_t \theta + (\mathbf{v} \nabla) \theta = \tau^{-1} R(\theta) + \kappa \nabla^2 \theta, \quad (1.2)$$

where \mathbf{v} is the flow velocity, p is the pressure, and θ represents temperature variations and/or the chemical composition of the fluid. It is convenient to choose θ equal to zero in the cold (heavy) phase and to unity in the hot (light) phase. Often, θ is referred to as the reaction progress variable. The reaction and production of heat is represented by the first term on the right hand side of Eq. (1.2); we refer to $R(\theta)$ as the reaction rate function, and to τ as the characteristic reaction time, or reaction time scale. We consider a single step reaction (see Poinso & Veynante 2005), where the reaction rate is zero in the pure phases, i.e. $R(0) = R(1) = 0$ and $R = O(1)$ for $0 < \theta < 1$. The buoyancy force, i.e. the last term on the right hand side of Eq. (1.1), is directed along the gravitational acceleration \mathbf{g} . The factor $\mathcal{A} = (\rho_1 - \rho_2)/(\rho_1 + \rho_2) \ll 1$ is the Atwood number, where

ρ_1 and ρ_2 are densities of the reactant and the product, respectively. We assume that the kinematic viscosity ν in Eq. (1.1) and the diffusion coefficient κ in Eq. (1.2) are comparable, and thus the Prandtl number is of the order of unity.

We compare our simulations with the benchmark non-reacting case, corresponding to $\tau = +\infty$ in Eq. (1.2). Phenomenological theory introduced by Chertkov *et al.* (2003; 2005) and hereafter called the “phenomenology” suggests that in the non-reacting RT turbulence, velocity and density fluctuations are driven by buoyancy at the scales L_v and L_θ , respectively, both comparable to the mixing zone width, H . These fluctuations generate cascades (of energy and temperature) towards small scales. The cascades terminate at the viscous scale, η , and (thermal) diffusive scale, r_d , respectively (Chertkov 2003; Chertkov *et al.* 2005). The scales η and r_d are of the same order provided the Prandtl number is of order unity. Previously conducted simulations of the non-reactive RT turbulence in the Boussinesq regime (Vladimirova & Chertkov 2008) show that while the mixing zone width grows in time, η and r_d decrease with time. It was also found that the correlation radii of both the velocity and temperature fluctuations, L_v and L_θ grow in time as $0.05\text{--}0.1H$. One special focus was on resolving the internal structure of the mixing zone more systematically than in the previous studies. It was shown that spatial correlations do not depend much on the vertical position within the mixing zone. In particular, this means that the relevant values of the major scales characterizing a snapshot of the RT turbulence depend only weakly on the height of the horizontal slice within the mixing zone.

2. Preliminary Considerations

In this paper we discuss the regime of relatively slow reaction: the time scale of the non-reacting RT instability, t_{inst} , and the characteristic reaction time, τ , are assumed to be well separated, $\tau \gg t_{\text{inst}}$.

At the early stage, $t < \tau$, development of the mixing zone and the range of turbulent scales inside the mixing zone are weakly influenced by the reaction. Nevertheless a cumulative effect of the reaction can be seen in the overall shift of the mixing zone, as a whole, from the product side to the reactant side. To estimate the shift of the mixing zone, z_f , let us integrate Eq. (1.2) along z . For the first term on the left hand side one arrives at $\partial_t z_f$, while the only other nonzero contribution is associated with the reaction term R/τ on the right hand side. Since in this regime the heat production is determined mainly by the mixing on the scale of the whole mixing layer, the reactive contribution is estimated simply as H/τ . Thus, $\partial_t z_f \sim H/\tau$. Even though the overall shift of the mixing zone at $t < \tau$ is smaller than H , z_f grows faster than H , so that the two scales become comparable at $t \sim \tau$. From this time onward the reaction effects become more prominent.

The reaction becomes more effective when the turbulent turnover time at H , estimated as t , exceeds the characteristic reaction time τ . In this regime the reactant entrained into the mixing zone is burned out completely, and the overall shift of the mixing zone, z_f , should be of order H . This transition in the mixing zone evolution is also accompanied by a qualitative modification of the temperature fluctuations in the interior of the mixing zone. In contrast, the velocity distribution at all the scales is expected to show only weak sensitivity to the reaction even at $t > \tau$.

The two stages observed for $t < \tau$ and $t > \tau$ will be called the *mixed stage* and the *segregated stage*, respectively. In the field of turbulent combustion (see Williams 1985; Peters 2000), the mixed regime is called “well-stirred reactor” (Poinsot & Veynante 2005), “thickened flame” (Borghi 1988) or “broken reaction zone” (Peters 2000) while the segregated regime is the regime of “distributed reaction zones” (Poinsot & Veynante 2005),

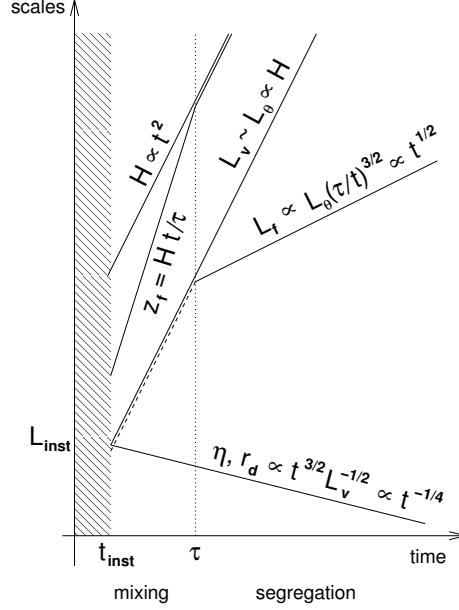


FIGURE 1. Schematic representation of the system evolution in log-log coordinates: the width of the RT mixing layer H , the large scale fluctuations of velocity and temperature L_v and L_θ , the shift of the mixing layer z_f due to reaction, the turbulent flame thickness L_f , and the dissipation scales η and r_d . The stages of the early RT instability development and transition to turbulence are shown shaded. τ is the characteristic reaction time, separating well-mixed and segregated regimes. In the mixed regime, the turbulent flame thickness corresponds to the typical width of interfaces, separating pure phase domains of size L_θ . The temporal scalings are phenomenological propositions discussed in Sections 2, 4.

“wrinkled-thickened flame” (Borghi 1988) or “thin reaction zone” (Peters 2000). Transition between the regimes occurring at $t \approx \tau$ can be interpreted as crossing the $Da = 1$ line on the turbulent combustion diagram (see Poinso & Veynante 2005). Indeed, the Damköhler number (Damköhler 1940), Da , is defined as the ratio of the integral time scale to the reaction time scale, $Da = t/\tau$, which grows linearly in time for the RT turbulence. The other popular dimensionless number in turbulent combustion, the turbulent Karlovitz number, Ka , describes transition between the regime of “distributed reaction zones”/“wrinkled-thickened flame”/“thin reaction zone” and the “flamelet” regime. The Karlovitz number is defined as the ratio of the chemical time scale to the Kolmogorov time scale. For the slowly reacting RT turbulence studied here, the “flamelet” regime does not apply, i.e. Ka is always much larger than unity and it increases with time. The laminar flame regime is also not observed in the systems considered here; consequently the laminar flame thickness h_{lam} is an irrelevant scale.

At $t > \tau$ the main effect of the reaction on the mixing zone is in creation of domains of pure phases ($\theta = 0$ and $\theta = 1$). In these domains the fluctuations in the reaction term of Eq. (1.1) dominate fluctuations in the respective advection term, leading to complete suppression (burning out) of temperature fluctuations. The domains are separated by relatively thin (compared to domain size) interfaces where burning occurs. The interface width, also referred to as the turbulent flame thickness, L_f , (that is the scale where the turnover time of velocity fluctuations is comparable to τ) becomes much smaller than L_v at $t \gg \tau$ due to the dominance of reaction.

Formation of the conglomerate of pure reactant and product domains should result

run	τ	h_{lam}	s_{lam}
A	1600.00	160.00	0.10
B	177.78	53.33	0.30
C	64.00	32.00	0.50
D	40.32	25.40	0.63
E	16.00	16.00	1.00

TABLE 1. Laminar flame parameter for simulations discussed in the text: reaction time τ , laminar flame thickness $h_{\text{lam}} = 4\sqrt{\kappa\tau}$, and laminar flame speed, $s_{\text{lam}} = 4\sqrt{\kappa/\tau}$, for KPP reaction.

in a qualitative transformation of the single-point statistics of the temperature field inside the mixing zone. A single peak distribution centered around $\theta = 1/2$ transforms into a distribution with two peaks, related to the emergence of pure phase domains corresponding to $\theta = 0$ and $\theta = 1$. The qualitative differences in the projected stages are summarized in Fig. 1 where the temporal behavior of different characteristics is shown schematically.

3. Numerical Results

The computational technique used in this work is similar to that described in Vladimirova & Chertkov (2008). In our simulations, we use the popular Kolmogorov-Petrovskii-Piskunov (KPP) model (Fisher 1937; Kolmogorov *et al.* 1937), where $R = 4\theta(1 - \theta)$ with $0 < \theta < 1$. The KPP model is not the only possible choice of the function $R(\theta)$. However, compared to other models, the KPP reaction provides a relatively thick laminar front which can be simulated at coarser resolution and makes computations more affordable. As before, we restrict ourself to the case of $\text{Pr} = 1$, and chose the units where $\nu = \kappa = 1$ and $2Ag = 1$. The laminar flame parameters for five simulation sets discussed below are shown in Table 1.

We solved the equations (1.1,1.2) using the spectral element code developed by Tufo & Fischer (2001). We use elements of size 30^3 with 12 collocation points in each direction. The size of our computational domain is $960 \times 960 \times 1440$ physical units, or $384 \times 384 \times 576$ collocation points. We stop our simulation at time $t = 128$, when the width of the mixing layer approaches the size of the computational domain. The boundary conditions are periodic in the horizontal (x, y) directions and no-slip in vertical (z) direction. The initial conditions, taken at $t = 0$, include a quiescent velocity and a slightly perturbed interface between the domains, determined by $\theta = \theta_0(z + \delta)$. The function $\theta_0(z) = 0.5[1 + \tanh(0.4z)]$ describes the density profile across the interface and $\delta(x, y)$ is a perturbation having the spectrum with modes $18 \leq n \leq 48$ with spectral index 0. Here the spectral index refers to the exponent of the wave-number (see Ramaprabhu *et al.* 2005), and it describes the shapes of the perturbation spectra.

The least processed results of numerical simulations, snapshots of the temperature field θ , are shown in Fig. 2; they are quite informative for our intuition. In case A ($\tau = 1600$) the structure of the mixing layer is practically indistinguishable from the non-reacting case (see Vladimirova & Chertkov 2008), at least up to $t = 128$. In case C ($\tau = 64$) the reaction starts to influence the temperature distribution somewhere between $t = 64$ and $t = 96$, where we observe emergence of regions of pure phases. In case E ($\tau = 16$) reactants and products are well separated by relatively thin interfaces at $t = 32$. Thus,

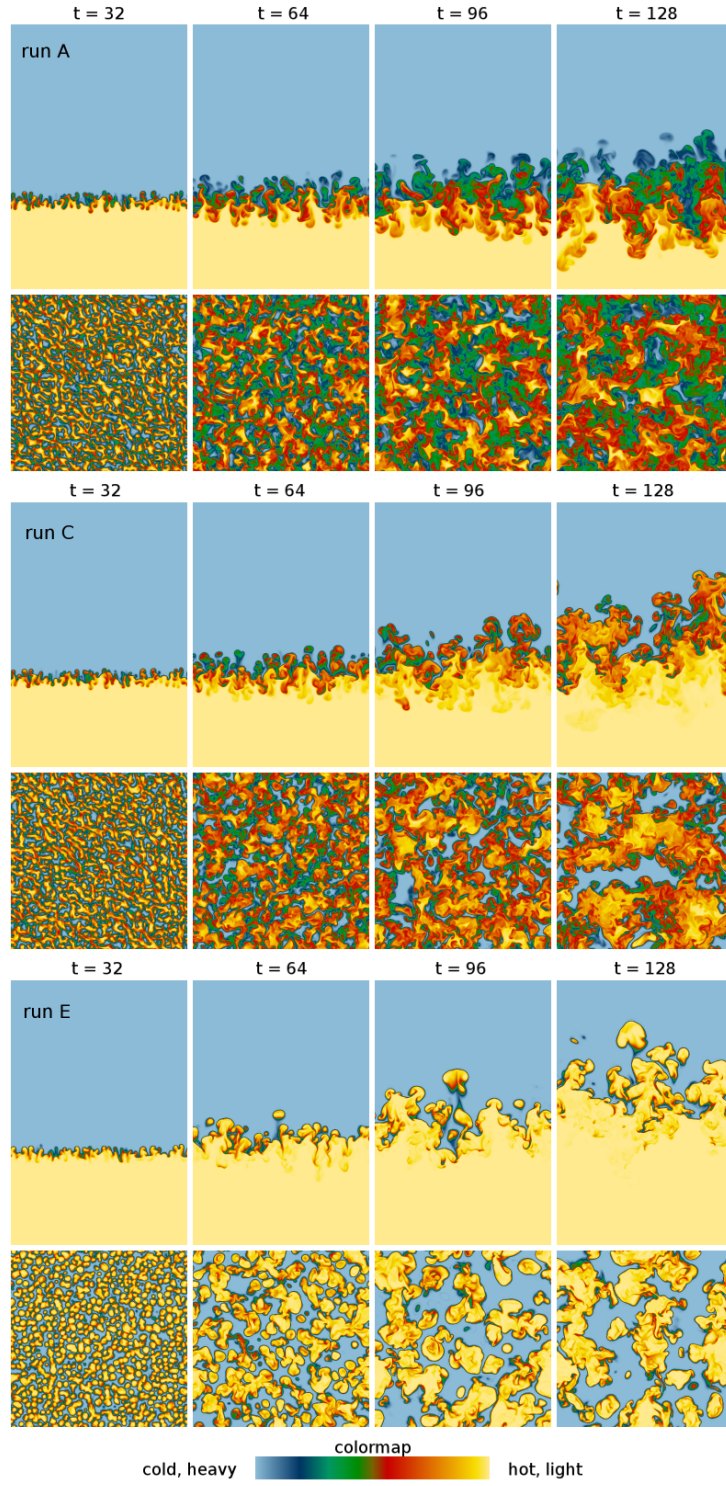


FIGURE 2. Vertical and horizontal ($z = z_f$, center of the mixing zone) slices of temperature for three different reaction strength.

a transition from the mixed stage to the segregated stage occurs at $t \approx \tau$, in accordance with the preliminary discussion of Section 2.

In Fig. 2 we observe that the width of the mixing layer, defined as the vertical distance between bubbles and spikes, is approximately the same in all cases. Measurements of the half-width of the mixing layer, defined as $H = \int \overline{R(\theta)} dz$ (where the overbar indicates averaging in a horizontal plane), confirm that $H(t)$ is weakly dependent on the reaction rate (see Fig. 3a). In Fig. 3b we plot the root mean square (RMS) of the vertical velocity and see that in all five cases the RMS velocity is practically the same. Moreover, all five cases exhibit similar internal structure of the velocity field inside the mixing layer, as we see from the comparison of the temperature and velocity correlation lengths, L_θ and L_v , measured in the central slice of the mixing zone (Fig. 3c). Following our earlier approach (Vladimirova & Chertkov 2008) we define the velocity correlation length, L_v , as the half-width of the normalized two-point pair correlation function of velocity, $f(0)/f(L_v) = 2$, with $f(r) = \langle v_z(\mathbf{r}_1)v_z(\mathbf{r}_1 + \mathbf{r}) \rangle / \langle v_z^2 \rangle$. The temperature correlation function is defined in a similar way, but based on the temperature fluctuations, $\theta - \bar{\theta}$. Both temperature and velocity correlation lengths differ by 20-30% compared to each other for τ ranging from 16 to 1600. Similarly to what was reported in Vladimirova & Chertkov (2008) for the non-reacting case, $L_\theta/H \approx L_v/H \approx 0.1$. The viscous length $\eta = (\nu^2 / \langle 5|\nabla v|^2 \rangle)^{1/4}$ decreases slowly with time in all cases, with less than 10% variation between $\tau = 16$ and $\tau = 1600$. The main conclusion here is that the velocity field is essentially insensitive to the reaction in the slow reaction regime.

Next we look at the shift of the mixing layer $z_f = \int \bar{\theta} dz$, introduced in Section 2. We compute the cumulative reaction, or bulk burning rate, $\dot{z}_f = \int \overline{R(\theta)} dz$, and compare it to the growth rate of the mixing layer, \dot{H} . Both quantities are shown as functions of time in Fig. 3d. We see that the bulk burning rate is greater for higher reaction rates. The time when \dot{H} and \dot{z}_f become comparable is approximately equal to τ .

It is not surprising that the bulk burning rate increases with decrease in τ . However, in addition to this obvious effect, we need to take into account the reaction efficiency, which depends on how well the fluids are mixed within the mixing layer. In Fig. 3e we show reaction efficiency of the whole mixing layer, $\dot{z}_f \tau / H$, and compare it to the reaction efficiency in the middle slice, $\bar{R}(z_f)$. Good agreement observed between the two characteristics suggests that the fraction of well-mixed fluid within the mixing zone does not vary significantly with the vertical position. In fact, we had also made this observation earlier in our study of the non-reacting case (Vladimirova & Chertkov 2008), where the mixing efficiency stayed at the constant level of ≈ 0.8 across the whole layer. In addition, Fig. 3e shows the fraction of well-mixed fluid, Δ_{mix} , defined as a relative area of the slice $z = z_f$ occupied by fluid with $0.25 < \theta < 0.75$. We see that Δ_{mix} behaves similar to $\bar{R}(z_f)$; some differences reflect an arbitrary choice of the selected limits. The area fraction Δ_{mix} , as well as the average reaction rate in the middle slice and the reaction efficiency characterize the transition from the mixed stage to the separated stage. In the mixed stage Δ_{mix} is of order unity, and in the segregated stage it is a decreasing function of time. Numerical results shown in Fig. (3e) confirm a decrease of Δ_{mix} observed for $t > \tau$.

Since the reaction at the central, $z = z_f$, slice describes the bulk burning rate so well, we pay particular attention to the temperature distribution within the slice, shown in Fig. 4. In case A the probability distribution function (PDF) of temperature evolves in time almost as if there were no reaction at all. It starts from a single peak distribution determined by the initial conditions (slightly perturbed diffused interface). Then, during the linear stage of the RT instability, $t \lesssim 16$, the PDF transforms into the two-peak shape and becomes single-peaked again at $t \approx 48$. The transformation from one to two peaks

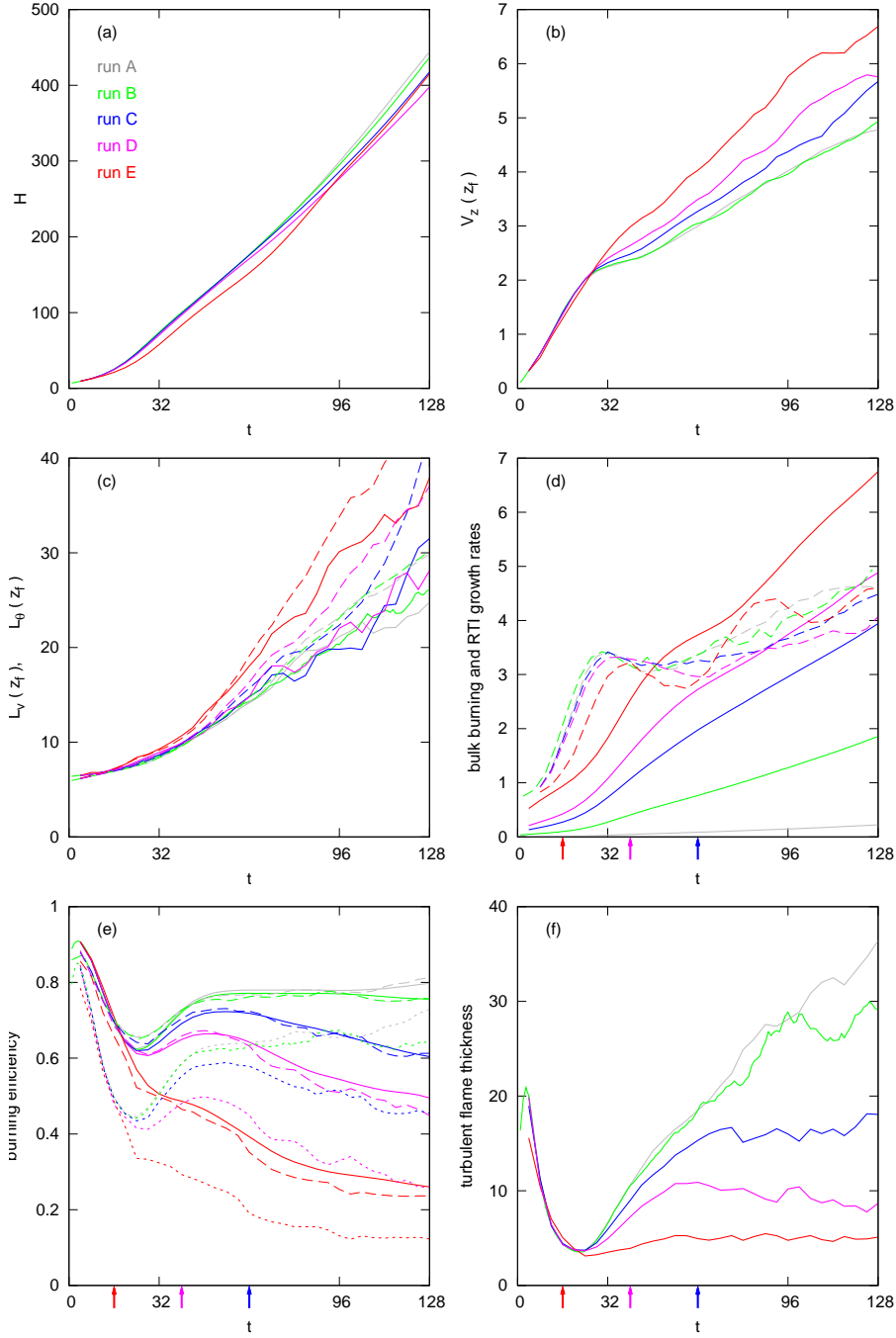


FIGURE 3. (a) half-width of mixing layer H ; (b) RMS of vertical velocity at z_f ; (c) pumping scale L_v (dashed lines) and scale L_θ (solid lines) measured at z_f ; (d) bulk burning rate \dot{z}_f (solid lines) compared to growth rate of RT instability \dot{H} (dashed dots); (e) burning efficiency measured as ratio $\dot{z}_f \tau / H$ (solid lines), the average reaction rate $\bar{R}(z_f)$ in the middle slice (dashed lines), and well-mixed fraction of the slice area, Δ_{mix} (dotted lines); (f) turbulent flame thickness in the middle slice obtained using “expanding circle” technique. Arrows in (d)-(f) show the reaction time.

corresponds to the transition to the non-linear regime of the RT instability, associated with secondary Kelvin-Helmholtz type shear instability and formation of RT mushrooms, while transition from two peaks to one corresponds to the destruction of RT mushrooms and formation of the turbulent mixed zone. When reaction is stronger, as in cases B and C, we observe yet another transformation in the PDF, namely the appearance of a narrow peak around $\theta = 0$ and decrease in the middle of the θ range at $t \approx \tau$. The transition to the two-peaked shape at $t \approx \tau$ is of interest to us since it indicates transition to the segregated regime. (In cases D and E, this 1-2-1-2 peak pattern is not noticeable because τ is of the order of, or shorter than, the transition time from linear to non-linear RTI.) Quantitatively the process of the transition to the segregated regime can be described by integrating the PDF function over some interval in the vicinity of $\theta = 1/2$. Selecting the interval $0.25 < \theta < 0.75$, we obtain Δ_{mix} , described earlier.

The well-mixed fraction, Δ_{mix} , is related to the turbulent flame width, L_f , or the width of the layer separating the pure-phase domains. Aiming to study the geometry of the turbulent flame we measure L_f in the following way: for each point with $1/4 < \theta < 3/4$ we find the largest radius of the circle around this point containing only points with $1/4 < \theta < 3/4$; this length, averaged and multiplied by four, represents the typical width of the burning region, L_f , shown in Fig. 3f. We observe that (i) L_f increases with τ , (ii) $L_f \sim L_\theta$ for $t < \tau$ (compare Fig. 3f and Fig. 3c), and (iii) for $t > \tau$, L_f grows with time but slower than L_v , so L_f/L_v decreases with time.

To summarize, we have observed in our numerics the transition at $t \approx \tau$ from mixed to segregated regimes in variety of ways, from visual comparison of temperature fields and temperature PDFs to direct measurements of reaction efficiency and turbulent flame thickness.

4. Phenomenology

This Section focuses on analysis of the asymptotic ($t \gg \tau$), segregated regime, supposedly characterized by extended inertial interval and scaling behaviors. The simulations discussed above do not run long enough to reach and accurately resolve this regime. However, the simulations are in a qualitative agreement with the phenomenology constructed, thus providing a starting point for more ambitious simulations in the future.

We first review the relevant facts from *non-reacting* RT turbulence, ($\tau = \infty$). In this case the phenomenology (Chertkov 2003), supported by numerical simulations (Cabot & Cook 2006; Zingale *et al.* 2005) and some (though limited) experimental observations, can be summarized as follows. At $t \gg t_{\text{inst}}$ the width of the mixing zone grows as $H \propto t^2$. Velocity fluctuations within the mixing zone are described by the Kolmogorov cascade, whereas temperature fluctuations follow the Corrsin-Obukhov cascade. Both cascades are driven by the largest RT scale (the spikes and bubbles) at $L_v \approx L_\theta \propto H$. Even though this driving scale grows with time, turbulence at smaller scales is adiabatically adjusted to the growth. The adiabaticity is due to the monotonic decrease of the turbulence turnover time with the scale.

As discussed above and illustrated in Fig. 1, for $t < \tau$ the development in the reacting case proceeds as in the benchmark non-reacting case. Here θ is well mixed within the mixing zone, and the single point distribution of the temperature is peaked around the median value of $\theta = 1/2$. Typical fluctuations of the velocity and temperature inside the mixing zone (measured in terms of the differences $\delta_r v$ and $\delta_r \theta$ between two points separated by a distance r) are described by the Kolmogorov-Corrsin-Obukhov estimates

$$\delta_r v \sim (L_v/t)(r/L_v)^{1/3}, \quad \delta_r \theta \sim (r/L_v)^{1/3}, \quad \text{if } L_v \gg r \gg \eta, r_d; \quad (4.1)$$

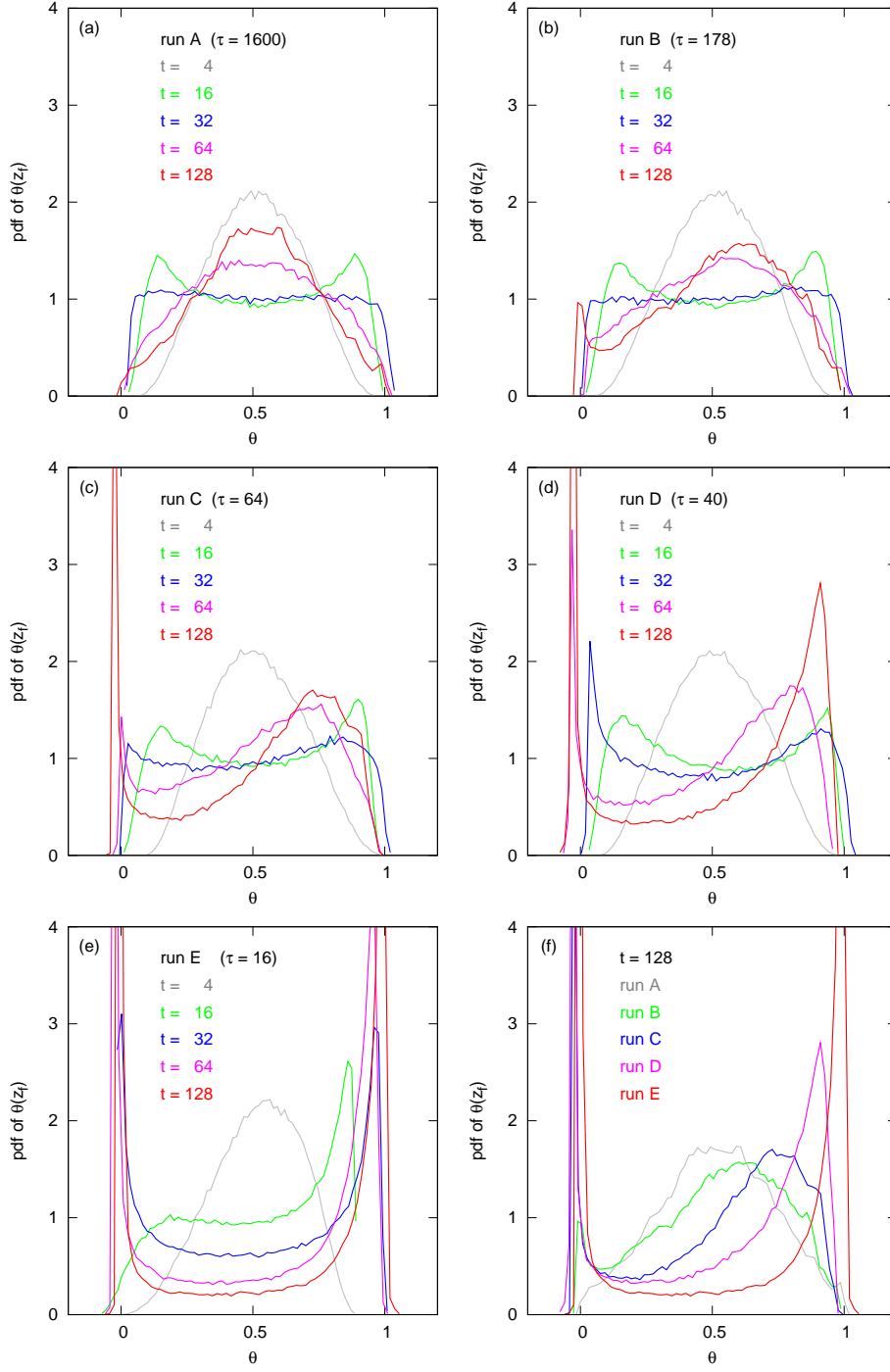


FIGURE 4. PDF of temperature in the middle slice. Panels (a)-(e) show time evolution of PDFs. Panel (f) compares PDFs at $t = 128$ for different reaction times, τ .

which are insensitive to the reaction. The viscous and thermal diffusion scales, η and r_d , can be estimated as $\eta \sim r_d \sim (\nu t)^{3/4}/L_v^{1/2} \propto t^{-1/4}$, provided the Prandtl number is of order unity.

Since the velocity correlation functions are formed by the direct cascade determined by the non-linear term in Eq. (1.1), the driving effectively occurs at the scale $L_v \approx L_\theta$, with the former one being not very sensitive to the reaction statistics, and thus determined by the same estimates as in the non-reacting case, Eq. (4.1). (Weak sensitivity of the velocity statistics to the reaction was also observed in our simulations, see Fig. 3.) In contrast, the θ statistics are strongly modified at $t \gg \tau$ when pure phase regions are formed separated by relatively thin interfaces (see Figs. 3 and 4). The interface width L_f is estimated by balancing advection and reaction terms in Eq. (1.2), $\delta_r v \delta_r \theta / r \sim \delta_r \theta / \tau$. One thus derives the following estimate for the turbulent flame thickness,

$$L_f \sim L_\theta (v_{L_\theta} \tau / L_\theta)^{3/2} \sim g \tau^{3/2} t^{1/2}. \quad (4.2)$$

The turbulent flame thickness does grow with time, but in such a way that both L_θ/L_f and L_f/r_d also grow as time advances. (Although our numerical data do not run long enough to illustrate the increase of L_f with time, we did observe the increase of L_f with τ . See Fig. 3f.)

Let us now exploit the Kolmogorov-Obukhov relation, calculating the time derivative of $\theta(\mathbf{r}_1)\theta(\mathbf{r}_2)$ in accordance with Eq. (1.2), and then averaging the result over a slice perpendicular to the Z -axis for a fixed value of $\mathbf{r} = \mathbf{r}_1 - \mathbf{r}_2$, where $L_f \ll r \ll L$. Making use of the adiabaticity and neglecting the reactive and diffusive terms in Eqs. (1.1,1.2) one derives

$$\nabla \langle (\mathbf{v}(\mathbf{r}_1) - \mathbf{v}(\mathbf{r}_2))(\theta(\mathbf{r}_1) - \langle \theta(\mathbf{r}_1) \rangle)(\theta(\mathbf{r}_2) - \langle \theta(\mathbf{r}_2) \rangle) \rangle \sim \varepsilon_\theta,$$

where the flux term on the right-hand side originates from driving at the large-scale, $v_z \partial_z \langle \theta \rangle$, due to the large scale temperature gradient set by buoyancy (Shraiman & Siggia 1994). Using the Kolmogorov estimation (4.1) for $\delta_r v$, one arrives at

$$S_2(r) \equiv \langle (\delta_r \theta)^2 \rangle \sim \varepsilon_\theta \varepsilon_v^{-1/3} r^{2/3} \sim (r/H)^{2/3}. \quad (4.3)$$

The most important assumption, made while deriving Eq. (4.3), concerns neglecting the reactive contribution into the θ^2 balance. This assumption will be justified later in the Section.

At $r \gg L_f$, Eq. (4.3) also describes the probability for two points separated by r to fall in two distinct domains of $\theta \approx 0$ and $\theta \approx 1$, or vice versa. Exactly the same probabilistic arguments apply to a temperature structure function of any positive order, thus resulting in the asymptotic independence of the respective scaling exponent of the order:

$$S_n(r) \equiv \langle |\delta_r \theta|^n \rangle \sim (r/H)^{2/3}. \quad (4.4)$$

The expression implies strong intermittency of the temperature field, as the ratios $S_n/(S_2)^{n/2} \sim (H/r)^{(n-2)/3}$ all grow with scale at $n > 2$. Notice that these arguments also apply to the immiscible RT, of the type discussed in Chertkov *et al.* (2005).

The expressions (4.3, 4.4) suggest that the flame interface is fractal and, moreover, single-fractal (as opposed to multi-fractal, see e.g. discussion of Sreenivasan *et al.* (1989) and Kerstein (1991)). The fractalization of the flame is properly explained by dependence of the fraction, Δ_{mix} , of the mixing zone on the turbulence flame thickness, L_f . Taking Eqs. (4.3, 4.4) at $r \rightarrow L_f$, one estimates, $\Delta_{\text{mix}} \sim (L_f/H)^{2/3} \sim \tau/t$. This also implies that $z_f \sim H$, thus confirming the general conclusion made in Section 2.

Now we are ready to justify the approximation leading to Eq. (4.3). Let us estimate

contribution of the flame/reaction term, $\mu = \langle [\theta(\mathbf{r}_1) - \langle \theta(\mathbf{r}_1) \rangle] R(\mathbf{r}_2) \rangle / \tau$, into the aforementioned θ^2 balance relation. The product is non-zero only if \mathbf{r}_2 falls inside the interface. Then μ is much less than $\langle R \rangle / \tau$ since $\theta(\mathbf{r}_1) - \langle \theta(\mathbf{r}_1) \rangle$ is of order unity and it also has zero average. The average $\langle R \rangle$ is determined by the fraction of the well mixed region within the mixing zone, $\Delta_{\text{mix}} \sim (L_f/H)^{2/3}$. One concludes, that, indeed, $\mu \ll 1/t \sim \varepsilon_\theta$ at $r \gg L_f$, thus justifying the assumption made above in deriving Eq. (4.3) and subsequently Eq. (4.4).

Turning to discussion of the range of scales smaller than L_f but larger than r_d , one notices that the reaction term does not contribute to the θ^2 balance, as it is much smaller than the respective advection contribution. At these scales, where the direct effect of the reaction term is irrelevant and the Kolmogorov velocity estimates still survive, one expects that the Obukhov-Corrsin scaling, $\delta_r \theta \propto r^{1/3}$, applies. Matching the self-similar behavior with Eq. (4.4) at L_f , one derives the following scaling relation for the structure functions at $L_f \gg r \gg r_d$

$$S_n(r) \sim (L_f/H)^{2/3} (r/L_f)^{n/3}. \quad (4.5)$$

This formula allows a simple interpretation: the first term on the right hand side stands for the fraction of the well mixed region within the mixing zone, Δ_{mix} , where the reaction takes place, while the second term accounts for the Corrsin-Obukhov decay of correlations with the decrease in scale. The main contribution in the RHS of Eq. (4.5) comes from the interfacial domains, while contributions associated with pure phase domains, where $\theta \approx 0$ or $\theta \approx 1$, is much smaller.

5. Conclusions

In this manuscript we analyze the reactive RT turbulence in the case of a slow flame realized when the typical reaction time τ is larger then the time of RT instability development, t_{inst} . The RT instability leads to formation of the mixing zone at $t \sim t_{\text{inst}}$. Further development of the mixing zone is roughly split into the early turbulent stage, $\tau \gtrsim t \gtrsim t_{\text{inst}}$, characterized by well-mixed hot and cold phases, and the later stage, $t \gtrsim \tau$, where pure state phases are segregated. In the early stage, the system is only mildly sensitive to the reaction (flame), resulting in a slight shift of the mixing zone as a whole, but no visible feedback of the flame on velocity distribution. The velocity fluctuations are still insensitive to the reaction, at $t \gtrsim \tau$, however the temperature fluctuations become modified significantly. In this regime, burning takes place within thin interfaces separating large patches of pure phases. Our numerical simulations confirm the basic prediction of the transition at $t \approx \tau$. All the qualitative features expected from the transition are observed in the simulations. Given that our numerical resources were not sufficient for detailed analysis of the asymptotic, $t \gg \tau$, stage, we rely here on the phenomenology. Separation of the advective range for density fluctuations in two ranges, and formation of a single-fractal flame interface are our two main phenomenological predictions. This highly intermittent behavior of density fluctuations is in a great contrast with what was observed without reaction. These and other predictions of the phenomenology are subjects for juxtaposition with future numerical and laboratory experiments.

Notice that the general picture of mixing at $t > \tau$ discussed above is reminiscent of the immiscible turbulence discussed in Chertkov *et al.* (2005). In both cases large regions of pure phases are separated by thin interfaces. Viewed at the scales larger than the interface width, the interfaces are advected passively. Moreover, strong intermittency in the density fluctuations, reported above for the reactive case, also takes place in the setting of externally stirred (e.g. by gravity) immiscible turbulence.

Finally, our phenomenology also applies to other regimes of turbulent flames, e.g. those realized in combustion engines, where the turbulent flame width is positioned in between the integral scales of turbulence and the viscous/diffusive scales, $L_v, L_\theta \gg L_f \gg \eta, r_d$.

6. Acknowledgments

We wish to thank P. Fischer for the permission to use the Nekton code, A. Obabko and P. Fischer for the detailed help in using the code, and V.G. Weirs for useful comments. This work was supported by the U.S. Department of Energy at Los Alamos National Laboratory under Contract No. DE-AC52-06NA25396, under Grant No. B341495 to the Center for Astrophysical Thermonuclear Flashes at the University of Chicago, and RFBR grant 06-02-17408-a at the Landau Institute.

REFERENCES

- BOCKMANN, M. & MULLER, S. C. 2004 Coarsening in the buoyancy-driven instability of a reaction-diffusion front. *Phys. Rev. E* **70**, 046302/1–5.
- BORGHI, R. 1988 Turbulent combustion modelling. *Progress in Energy and Combustion Science* **14**, 245–292.
- CABOT, W. H. & COOK, A. W. 2006 Reynolds number effects on rayleigh-taylor instability with possible implications for type ia-supernovae. *Nature Physics* **2**, 562–568.
- CETEGEN, B. M. & KASPER, K. D. 1996 Experiments on the oscillatory behavior of buoyant plumes of helium and helium-air mixtures. *Phys. Fluids* **8**, 2974–2984.
- CHANDRASEKHAR, S. 1961 *Hydrodynamic and hydrodynamic instability*. New York: Dover Publications.
- CHERTKOV, M. 2003 Phenomenology of rayleigh-taylor turbulence. *Phys. Rev. Lett.* **91**, 115001/1–4.
- CHERTKOV, M., I., KOLOKOLOV, & LEBEDEV, V. 2005 Effects of surface tension on immiscible rayleigh-taylor turbulence. *Phys. Rev. E* **71**, 055301/1–4.
- COOK, A. W. & DIMOTAKIS, P. E. 2001 Transition stages of rayleigh–taylor instability between miscible fluids. *J. Fluid Mech.* **443** (2), 69–99.
- CORRSIN, S. 1951 On the spectrum of isotropic temperature fluctuations in an isotropic turbulence. *J. Appl. Phys.* **22**, 469–474.
- DALZIEL, S. B., LINDEN, P. F. & YOUNGS, D. L. 1999 Self-similarity and internal structure of turbulence induced by rayleigh-taylor instability. *J. Fluid Mech.* **399**, 1–48.
- DAMKÖLER, G. 1940 The effect of turbulence on the flame velocity in gas mixtures. *Z. Electrochem. Angew. Phys. Chem.* **46**, 601–626.
- DUFF, R. E., HARLOW, F. H. & HIRT, C. W. 1962 Effects of diffusion on interface instability between gases. *Phys. Fluids* **5**, 417–425.
- FISHER, R. 1937 The wave of advance of advantageous genes. *Annals of Eugenics* **7**, 355–369.
- FREEMAN, J. R., CLAUSER, M. J. & THOMPSON, S. L. 1977 Rayleigh-taylor instabilities in inertial-confinement fusion targets. *Nuclear Fusion* **17**, 223–230.
- FRISCH, U. 1995 *Turbulence. The Legacy of A. N. Kolmogorov*. Cambridge: Cambridge University Press.
- GAMEZO, V. N., KHOKHLOV, A. M., ORAN, E. S., CHTCHELKANOVA, A. Y. & ROSENBERG, R. O. 2003 Thermonuclear supernovae: Simulations of the deflagration stage and their implications. *Science* **299**, 77–81.
- KERSTEIN, A. R. 1991 Fractal dimensions of propagating interfaces in turbulence. *Phys. Rev. A* **44**, 3363–3365.
- KERSTEIN, A. R. 2001 Turbulence in combustion processes. *Proceedings of the Combustion Institute* **29**, 1763–1773.
- KHOKHLOV, A. M. 1995 Propagation of turbulent flames in supernovae. *Astrophys. J.* **449**, 695–713.
- KOLMOGOROV, A. N. 1941 The equation of turbulent motion in an incompressible viscous fluid. *Izv. Akad. Nauk. SSSR, Ser. Fiz.* **VI** (1-2), 56–58.

- KOLMOGOROV, A. N., PETROVSKII, I. G. & PISKUNOV, N. S. 1937 étude del'équation de la chaleur de matière et son application à un problème biologique. *Bulleten Moskovskogo Gosudarstvennogo Universiteta, Matematika i Mekhanika* **1**, 1–25, for an English translation see P. Pelcé, Ed. and Dynamics of curved fronts, Academic Press, 1988, pp. 105–130.
- LIMA, D., VAN SAARLOOS, W. & DE WIT, A. 2006 Rayleigh-taylor instabilities of pulled versus pushed fronts. *Physica D* **218**, 158–166.
- OBUKHOV, A. M. 1949 Structure of the temperature field in a turbulent flow. *Izv. Akad. Nauk SSSR, Geogr. Geofiz* **13**, 58–69.
- PETERS, N. 2000 *Turbulent Combustion*. Cambridge, UK: Cambridge University Press.
- POINSOT, T. & VEYNANTE, D. 2005 *Theoretical and numerical combustion*. Philadelphia: Edwards.
- RAMAPRABHU, P., DIMONTE, G. & ANDREWS, M. 2005 A numerical study of the unfluence of initial perturbations on the turbulent rayleigh-taylor instability. *J. Fluid Mech.* **536**, 285–319.
- RAYLEIGH, LORD 1883 Investigation of the character of the equilibrium on an incompressible heavy fluid of variable density. *Proc. of the London Math. Soc.* **14**, 170–177.
- RISTORCELLI, R. & CLARK, T. T. 2004 Rayleigh taylor turbulence: self-similar analysis and direct numerical simulation. *J. Fluid Mech.* **507**, 213–253.
- SHARP, D. H. 1984 An overview of rayleigh-taylor instability. *Physica D* **12**, 3–18.
- SHRAIMAN, B. & SIGGIA, E. 1994 Lagrangian path integrals and fluctuations in random flow. *Phys. Rev. E* **49**, 2912–2927.
- SREENIVASAN, K.R., RAMSHANKAR, R. & MENEVEAU, C. 1989 Mixing, entrainment and fractal dimensions of interfaces in turbulent flows. *Proc. Roy. Soc. Lond. A* **421**, 79–108.
- TAYLOR, G. 1950 The instability of liquid surfaces when accelerated in a direction perpendicular to their planes. *Proc. of the Royal Soc. of London. Series A, Mathematical and Physical Sciences* **201** (1065), 192–196.
- TIESZEN, S. R. 2001 On the fluid mechanics of fires. *Annual Review of Fluid Mechanics* **33**, 67–92.
- TUFO, H. M. & FISCHER, P. F. 2001 Fast parallel direct solvers for coarse grid problems. *J. Parallel Distr. Comput.* **61**, 151–177.
- VLADIMIROVA, N. & CHERTKOV, M. 2008 Self-similarity and universality in rayleigh-taylor boussinesq turbulence. *submitted to Phys. Fluids* LANL Preprint: LAUR-07-1669.
- VLADIMIROVA, N. & ROSNER, R. 2005 Model flames in the boussinesq limit: The case of pulsating fronts. *Phys. Rev. E* **71**, 067303/1–4.
- WILLIAMS, F. A. 1985 *Combustion theory*. Menlo Park, CA: Benjamin Cummings.
- WILSON, P. N. & ANDREWS, M. J. 2002 Spectral measurements of rayleigh-taylor mixing at small atwood number. *Phys. Fluids* **14**, 938–945.
- YOUNG, Y. N., TUFO, H., DUBEY, A. & ROSNER, R. 2001 On the miscible rayleigh-taylor instability: two and three dimensions. *J. Fluid Mech.* **447**, 377–408.
- ZINGALE, M., WOOSLEY, S. E., RENDLEMAN, C. A., DAY, M. S. & BELL, J. B. 2005 Three-dimensional numerical simulations of rayleigh-taylor unstable flames in type ia supernovae. *Astrophys. J.* **632**, 1021–1034.